

The Waterborne Superamphiphobic Coatings with Antifouling, High Temperature Resistance, and Corrosion Resistance

Guoyu Ren,^{*} Zeting Qiao, Zhi Hui, Yun Tuo, Wenjie Zheng, Xiaodong Chen, and Shiyong LiCite This: *ACS Omega* 2023, 8, 13578–13592

Read Online

ACCESS |



Metrics & More

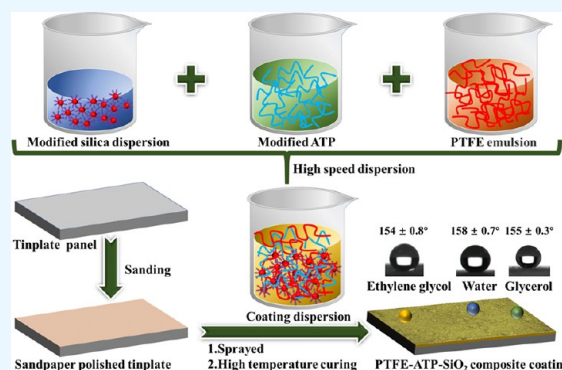


Article Recommendations



Supporting Information

ABSTRACT: Water-based superamphiphobic coatings are environment-friendly, which have attracted tremendous attention recently, but the performances are severely limited by the dispersibility of hydrophobic particles. To solve the poor dispersibility of modified silica powder with hydrophobicity, silica dispersion was blended with polytetrafluoroethylene (PTFE) emulsion and modified aluminum tripolyphosphate (ATP) dispersion to successfully prepare water-based coatings. Multifunctional coatings were prepared by one-step spraying. It possessed good adhesion (grade 1), excellent antifouling, impact resistance, chemical stability (acid and alkali resistance for 96 h of immersion), and corrosion resistance (3.5 wt % NaCl solutions for 20 days). More importantly, the superamphiphobic coatings had high contact angles (CAs) and low slide angles (SAs) for ethylene glycol (CAs = $154 \pm 0.8^\circ$; SAs = $13 \pm 0.7^\circ$) and water (CAs = $158 \pm 0.7^\circ$; SAs = $4 \pm 0.3^\circ$). Furthermore, the composite coating was still hydrophobic after 35 cycles of wear with high roughness sandpaper (120 mesh) under three different loads, which maintained superamphiphobicity at 425°C . This work is expected to provide a facile idea and method for the preparation of waterborne superamphiphobic coatings.



1. INTRODUCTION

The study of superamphiphobic surfaces originated from bionics, and oil-repellent organisms on the surface were found in nature,¹ such as bacterial biofilm (*Bacillus subtilis*),² leafhopper skin,³ fish skin, and springworm skin.^{4–6} Inspired by nature, researchers have attempted to develop superamphiphobic coatings to solve industrial problems.⁷ Due to excellent water and oil repellency, superamphiphobic coatings are widely used in self-cleaning,⁸ antifouling,⁹ anti-icing,¹⁰ drag reduction,¹¹ anticorrosion,¹² chemical shielding,¹³ and crude oil transportation.¹⁴ The micro/nanostructures and low surface energy chemistry are inseparable factors for obtaining superamphiphobic coatings.^{15–18} To obtain superamphiphobic coatings with excellent performances, volatile organic compounds (VOCs) are generally used to a disperser to enhance the dispersion of coatings, such as toluene,^{19,20} acetone,^{21,22} ethyl acetate,²³ and dichloropentafluoropropane.²⁴ They are harmful to the environment and human health. In recent years, the preparation of environment-friendly waterborne superamphiphobic coatings attracted researchers' interest. However, it seemed contradictory to disperse hydrophobic substances in water, which tended to float on the water surface.²⁵ Poor dispersion will lead to the low performance of superhydrophobic coatings, and it is not easy to realize oil repellency on the surface. Therefore, improving the dispersion of the waterborne coating will be conducive to replacing solvent superhydrophobic and oil repellent coatings.

At present, a lot of work has been done to solve dispersibility, and many researchers have made attempts. Some studies have reported simple methods for obtaining dispersions of aqueous superhydrophobic coating by dispersing silica particles in silane/siloxane/organic polymer waterborne emulsion and coating on different substrates to obtain superhydrophobic surfaces.^{26–30} Although these waterborne superhydrophobic coatings were prepared by various methods to enhance the dispersion of coatings, there were few reports on the exploration of dispersion stability. In the preparation methods of a rough surface, some reports had chemically etched the surface of aluminum alloy with $\text{HNO}_3/\text{HCl}/\text{HF}$,^{31,32} CuCl_2 ,³³ and NaOH solution.³⁴ It had been treated with low surface energy materials to fabricate the superamphiphobic surfaces. Chemical etching avoided harmful VOCs, but acid and alkali solutions endangered human health and affected the mechanical properties of the alloy to a certain extent. Zhang et al. prepared the dispersion of tetraethyl orthosilicate (TEOS), 1H,1H,2H,2H-perfluorodecyltriethoxy-

Received: October 24, 2022

Accepted: March 24, 2023

Published: April 4, 2023



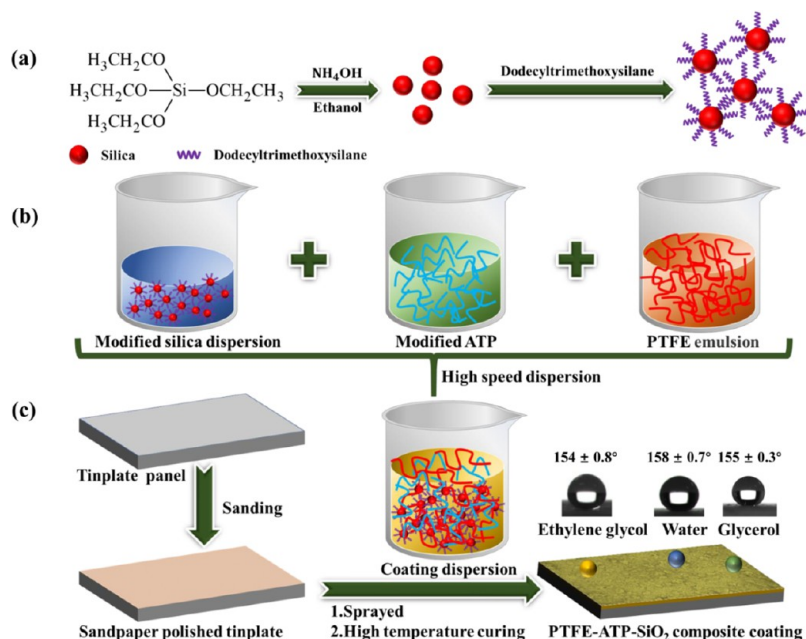


Figure 1. Schematic illustration of the preparation procedures. (a) Schematic diagram of preparation of modified silica nanoparticles. (b) Preparation process of the PTFE-ATP-SiO₂ composite coating dispersion. (c) Film forming process of the PTFE-ATP-SiO₂ composite coating.

silane (PFDTES), and nanosilica by improving the Stöber method and then sprayed it on an AA5083 alloy substrate to obtain superamphiphobic coatings.³⁵ Although the dispersion of superamphiphobic coatings with excellent dispersibility was fabricated by one pot, the wear resistance of the surface has not been discussed. In addition, the stability was not explored. Li et al. used a four-step spraying method to successively form a coating system of polyurethane, silica fluoride, methyl silicone, and silica fluoride, which obtained superamphiphobic surfaces with excellent performance.³⁶ However, the preparation steps are too cumbersome.

In this study, dodecyltrimethoxysilane was used to modify silica, which reduced the hydrophilic groups of nanosilica and enhanced the hydrophobicity. Compared with the zeta potential of silica dispersion (0.1 g/L, 17.45 ± 0.95 mV), the zeta potential of modified silica dispersion (0.1 g/L, 32.8 ± 0.9 mV) was larger due to the steric hindrance of dodecyltrimethoxysilane on the silica surface.^{37–39} Therefore, the modified silica dispersion was more stable. To solve the dispersibility of hydrophobic particles, silica dispersion was blended with polytetrafluoroethylene (PTFE) emulsion and modified aluminum tripolyphosphate (ATP) dispersion to successfully prepare water-based dispersion. The water-based dispersion was sprayed and cured at 320 °C to fabricate superamphiphobic surfaces. It obtained excellent moisture resistance for ethylene glycol (CAs = 154 ± 0.8°; SAs = 13 ± 0.7°) and water (CAs = 158 ± 0.7°; SAs = 4 ± 0.3°). Furthermore, the polytetrafluoroethylene-modified aluminum tripolyphosphate-modified silica (PTFE-ATP-SiO₂) composite coating possessed good adhesion (grade 1), thermal stability (<425 °C), excellent antifouling, and impact resistance. More importantly, the modified ATP improved the density of the PTFE-ATP-SiO₂ composite coating and was regarded as an anticorrosive material to enhance corrosion resistance.^{40,41} After 20 days of immersion in 3.5% NaCl solution, the PTFE-ATP-SiO₂ composite coating still had 89.1% protection efficiency. This work is expected to provide a facile idea and method for the preparation of waterborne superamphiphobic

coatings with high temperature resistance and anticorrosion by one-step spraying.

2. EXPERIMENTAL SECTION

2.1. Materials. Hydrochloric acid and potassium hydroxide were purchased from Tianjin Kemio Chemical Reagent Co., Ltd. (China). PTFE emulsion (60 wt %, TE3893) was provided by DuPont (USA). Tetraethyl orthosilicate was provided by Tianjin Damao Chemical Reagent Factory (China). Ammonia and anhydrous ethanol were purchased from Tianjin Tianli Chemical Reagent Co., Ltd. (China). Modified aluminum tripolyphosphate (P₂O₅: 48–52 wt %; Al₂O₃: 11–14 wt %; ZnO: 18–22 wt %) was from Shandong Yousuo Chemical Technology Co., Ltd. (China). Dodecyltrimethoxysilane was supplied by Nanjing Youpu Chemical Co., Ltd. (China). Sodium chloride and glycerol were purchased from Tianjin Zhiyuan Chemical Reagent Co., Ltd. (China).

2.2. Preparation of Modified Silica Nanoparticles. The preparation process of modified silica nanoparticles is shown in Figure 1a. Silica was prepared by the Stöber method⁴² and modified by dodecyltrimethylsilane with a low surface material to reduce the hydroxyl groups and enhance the hydrophobicity. The preparation steps are as follows. A mixed solution (250 mL) of ammonia:anhydrous ethanol:deionized water in the ratio of 1:7:2 was added to a 500 mL three-necked flask and stirred at 45 °C. Tetraethyl orthosilicate (45 g) was evenly mixed with 15 mL of deionized water. Also, the tetraethyl orthosilicate solution was slowly added into the mixed solution. The silica sol was obtained by continuous and uniform stirring at 45 °C for 3 h. Dodecyltrimethylsilane (20 g) was added into the silica sol and stirred evenly for 2 h to obtain the modified silica sol. Deionized water was added to the above sol and centrifuged by a high-speed centrifuge.

2.3. Preparation of the Composite Coating. The surface of the tinplate was polished with 120-mesh sandpaper in one direction for 4 min and polished vertically for 4 min to

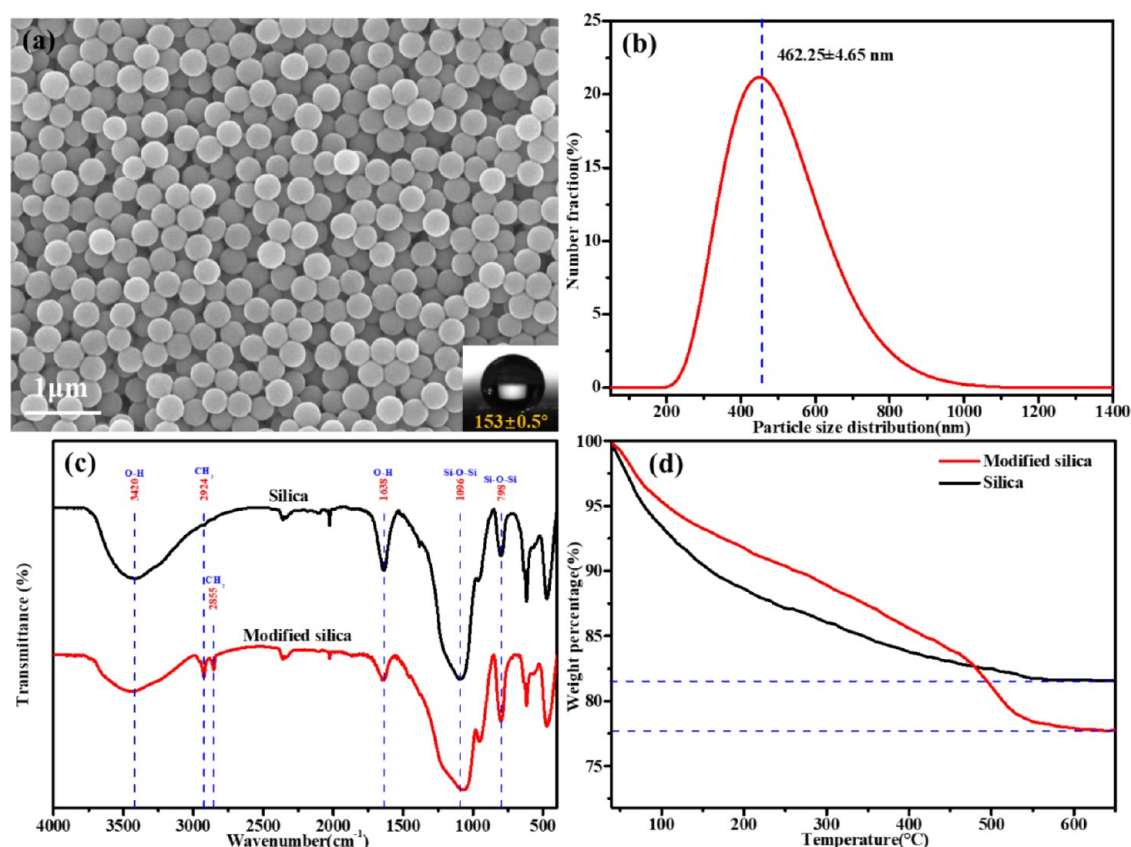


Figure 2. Characterization of modified silica nanoparticles. (a) SEM and CAs of modified silica nanoparticles. (b) Particle size distribution. (c) FT-IR spectra. (d) Thermogravimetry of modified silica nanoparticles.

remove oil and rust. Then, the residue was blown away with a blower for standby. As shown in Figure 1b, it was the preparation process of the coating dispersion. Modified silica particles (25 g, 90 wt %), modified ATP (50 g, 20 wt %), and PTFE emulsion (50 g, 60 wt %) were evenly stirred for 1 h under a high-speed stirrer to obtain the coating dispersion. As shown in Figure 1c, it was the film-forming process. The obtained coating dispersion was transferred to a spray can, which evenly sprayed on the sandpaper polished tinplate at a pressure of 4 bar, and then cured at 320 °C in a high-temperature oven for 20 min to prepare superamphiphobic surfaces.

2.4. Characterization. The modified silica particles were characterized by a field emission scanning electron microscope (Sigma 300), in situ infrared spectrometer (Bruker Tensor 27), and synchronous thermal analyzer (LABSYS EVO). A zeta potential analyzer (Malvern Zetasizer Nano ZS90) was used to obtain the zeta potential and particle size distribution. The CAs and SAs were measured by a contact angle meter (JC2000C1, Shanghai Zhongchen Digital Technology Equipment Co., Ltd.). Five microliter samples (deionized water, ethylene glycol, glycerol, hydrochloric acid solution, and potassium hydroxide solution) were measured. Also, each measurement needed to test five parts of the sample surface and take the average value.

The morphology and element composition of the composite coating were observed by a field emission scanning electron microscope (Sigma 300). The 3D surface morphology and thickness of the composite coating were obtained by a 3D profiler (KLA-Tencore, D-120). The composite coating was analyzed by an X-ray diffractometer (Bruker D8 Advance) and

in situ infrared spectrometer (Bruker Tensor 27). According to GB/T 6739, the composite coating was tested by a pencil hardness tester to evaluate film hardness (QH-Q type, Dongguan Huaguo Precision Instrument Co., Ltd.). A cross-cut tape test of the composite coating was conducted to evaluate the adhesion according to GB/T 9286. According to GB/T 1732, the impact resistance of the composite coating was tested by a paint film impact instrument (QCJ-50/100, Tianjin World Expo Weiyi Chemical Glass Instrument Co., Ltd.). An electrochemical workstation was adopted to conduct the electrochemical corrosion measurement in 3.5 wt % NaCl solution (CHI760E, Shanghai Chenhua Instrument Co., Ltd.).

3. RESULTS AND DISCUSSION

3.1. Analysis of Modified Silica Nanoparticles. The prepared modified silica nanoparticles are shown in Figure 2a. The appearance was uniformly spherical, and the CAs of particles were $153 \pm 0.5^\circ$ for deionized water. The average particle size was 462.25 ± 4.65 nm (Figure 2b). Compared with silica, the infrared spectra of modified silica showed absorption peaks at 2855 cm^{-1} (symmetric stretching vibration peak) and 2924 cm^{-1} (antisymmetric stretching vibration peak), which belonged to methylene (CH_2) and methyl (CH_3), respectively. In addition, the hydroxyl absorption peaks at 1638 and 3420 cm^{-1} were weakened and hydrophilic groups were reduced compared with silica (Figure 2c).^{43–45} It indicated that silica was successfully modified by dodecyltrimethoxysilane. The mass percentage of silica-branched dodecyltrimethoxysilane was measured by a synchronous thermal analyzer. For modified silica, the additional weight

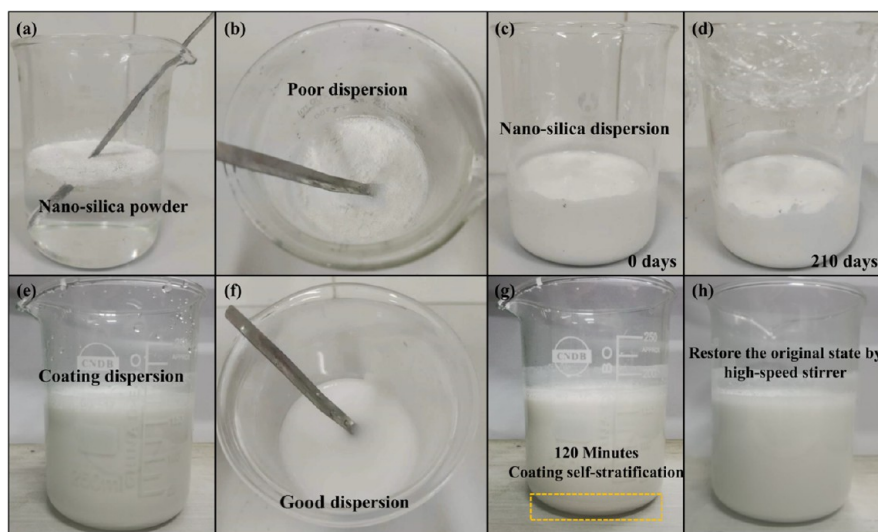


Figure 3. Dispersion stability. (a) Nanosilica powder suspended in water. (b) Nanosilica powder suspended in the coating dispersion. (c) Dispersion of modified silica nanoparticles. (d) Dispersion of modified silica nanoparticles after 210 days. (e, f) PTFE-ATP-SiO₂ composite coating dispersion. (g) PTFE-ATP-SiO₂ composite coating dispersion after 120 min. (h) PTFE-ATP-SiO₂ composite coating dispersion after high-speed dispersion again.

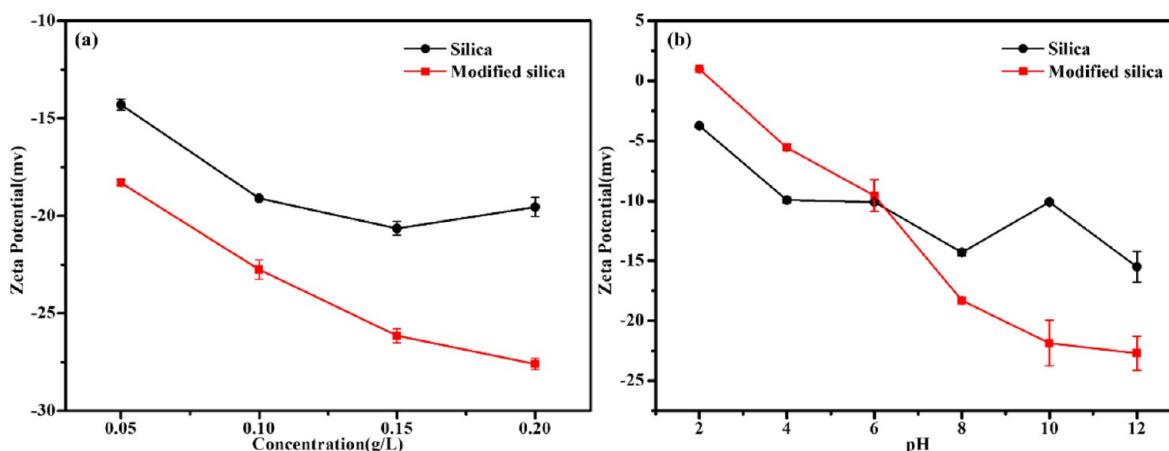


Figure 4. Zeta potential of coating dispersion. (a) Effect of concentration on zeta potential. (b) Effect of pH on zeta potential.

loss rate was about 3.91% compared with unmodified silica (Figure 2d).

3.2. Analysis of the Composite Coating Dispersion.

For water-based superamphiphobic coatings, dispersibility decides the performance. However, the hydrophobic substances often float on the water surface, resulting in poor dispersibility (Figure 3a,b). Therefore, we solved the dispersibility by preparing modified silica dispersion instead of modified silica powder and obtained water-based superamphiphobic dispersion (Figure 3e,f). The prepared modified silica dispersion was milky white (Figure 3c). When the dispersion of modified nanosilica was stored for 210 days, it was clearly found that the dispersion was not layered (Figure 3d). As shown in Figure 3g, it was layered when the coating dispersion was placed for 120 min, but the coating dispersion returned to the original state after passing through the high-speed stirrer (Figure 3h). In addition, the coating dispersion after redispersion does not affect the coating spraying and performance (Figure S1).

Silica dispersion has a large phase interface, so the colloidal particles are in an unstable state to be destroyed and

agglomerated.^{46,47} Consequently, the one-step synthesis and hydrophobic modification have been adopted to improve stability for fabricating the modified silica dispersion with excellent dispersibility. During the process of one-step synthesis of the modified silica dispersion, dodecyltrimethoxysilane was used to modify the surface of dispersed phase particles (silica), reduce the surface energy, and play a role in steric hindrance on the surface of silica.^{37–39} Zeta potential (absolute value) is usually an important index to evaluate the stability of the colloidal dispersion system.^{48,49} The silica dispersion with 437.2 ± 13.1 nm average particle size and the modified silica dispersion with 462.25 ± 4.65 nm average particle size were synthesized, it was found that the modified silica dispersion had a large zeta potential (0.1 g/L, 32.8 ± 0.9 mV), and its stability was better than that of the silica dispersion by comparing with the zeta potential of the silica dispersion (0.1 g/L, 17.45 ± 0.95 mV).

To evaluate the stability of the coating dispersion, the zeta potential of coating dispersions with different concentrations of silica (437.2 ± 13.1 nm) and modified silica (462.25 ± 4.65 nm) was measured (Figure 4a). It was found that with the

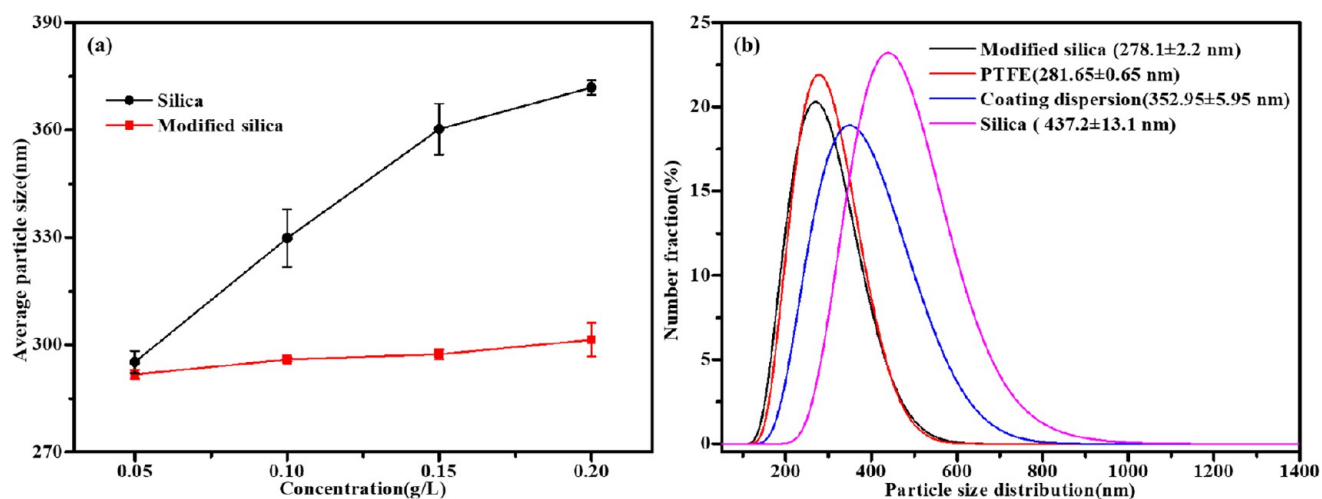


Figure 5. Particle size distribution. (a) Effect of concentration on the average particle size. (b) Particle size distribution of dispersion.

increase in concentration, the zeta potential of the coating dispersion increased, indicating that the stability increased. As shown in Figure 5a, with the increase in particle concentration, the average particle size of the coating dispersion prepared with modified silica increased relatively slowly, while the average particle size of the coating dispersion prepared with silica increased rapidly. The maximum difference in average particle size between the two was 70.45 nm. Therefore, compared with the coating dispersion prepared with modified silica, the coating dispersion prepared with silica was easier to accumulate. Furthermore, the zeta potential of modified silica was higher than that of silica, which indicated that the stability of the coating dispersion prepared with modified silica was good.

The zeta potential of coating dispersions prepared with silica (437.2 ± 13.1 nm) and modified silica (462.25 ± 4.65 nm) with different pH levels (2, 4, 6, 8, 10, and 12) was measured so as to explore the influence of pH on the stability of the coating dispersion (Figure 4b). The results showed that the zeta potential of the coating dispersion prepared with modified silica and silica under the alkaline condition was higher than that under the acidic condition, and alkaline condition was conducive to the stability of the coating dispersion. The composite coating dispersion included PTFE emulsion (pH 9–10), modified silica dispersion (neutral), and modified ATP dispersion (pH 6–7), of which PTFE emulsion was the main substance (Figure 8). Therefore, the stability of the composite coating dispersion was mainly determined by the stability of PTFE emulsion. For the stability of PTFE emulsion, it was determined by the synthesis process and stable environment (acid–base properties). In this paper, PTFE emulsion (TE3893) was an alkaline dispersion, so alkaline condition was conducive to improving the stability of the composite coating dispersion.

In addition, the effect of modified silica particle size on the stability of the coating dispersion was investigated. It was found that there was little difference in the zeta potential of the coating dispersion prepared with 278.1 ± 2.2 nm (0.1 g/L, 22.75 ± 0.15 mV) and 462.25 ± 4.65 nm (0.1 g/L, 23.25 ± 0.15 mV) modified silica. As shown in Figure 5b, compared with the coating dispersion with 462.25 ± 4.65 nm modified silica, the coating dispersion with 278.1 ± 2.2 nm modified silica had a larger particle size (352.95 ± 5.95 nm).

Consequently, small particle size was not conducive to the stability of dispersion and led to easier accumulation. To sum up, the modification, concentration, particle size, and pH have a great impact on the stability of the coating dispersion.

3.3. Analysis of Wettability of the Composite Coating

Since the coating dispersion was composed of PTFE, modified silica nanoparticles, and modified ATP, weight percentages of modified silica nanoparticles and modified ATP were changed to explore the influence on the wettability of coating. Under the condition of 50 g of PTFE emulsion (60 wt %) and 50 g of modified ATP (20 wt %), the amount of modified silica was changed (five kinds of formulations). It was obvious that the waterproof ability of the coating can be improved by adding modified silica nanoparticles (Figure 6a,b). When the weight percentage of modified silica nanoparticles was 36 wt % (25 g), the maximum CA of water reached 158.7° , and the CAs of ethylene glycol were $151 \pm 0.6^\circ$. When the weight percentage of modified silica nanoparticles was 40.3 wt % (30 g), the composite coating had the maximum CA (154.8°) for ethylene glycol, the CAs of water were $155 \pm 1^\circ$ (Figure 6a). When the weight percentage of modified silica nanoparticles changed from 18.37 wt % (10 g) to 47.37 wt % (40 g), the SAs of water were transformed from $9 \pm 0.2^\circ$ to $3 \pm 0.1^\circ$, and the SAs were changed from $17.9 \pm 0.6^\circ$ to $13 \pm 0.5^\circ$ for ethylene glycol. With the amount of filled modified silica increasing, the composite coating surface easily formed an inhomogeneous rough structure and had high apparent contact angle. It conformed to the Cassie–Baxter model.⁵⁰ In the Cassie–Baxter model, it was assumed that the droplet only contacts with the solid tip (inhomogeneous surface) and intercepts air in an inhomogeneous rough structure under the droplet so that the inhomogeneous surface is not wetted. The apparent contact angle increased with the decrease in the contact between the droplet and the solid tip, which was basically consistent with our experimental results (Figure S2). Therefore, under the quantitative condition of PTFE (50 g) and modified ATP (50 g), the composite coating with 36 wt % (25 g) modified silica nanoparticles obtained high CAs. Then, the amount of modified ATP was optimized, which was changed under the dosage of 50 g of PTFE emulsion (60 wt %) and 25 g of modified silica (90 wt %). Five kinds of formulations were evaluated (Figure 6c,d). When the weight percentage of modified ATP was changed from 10.26

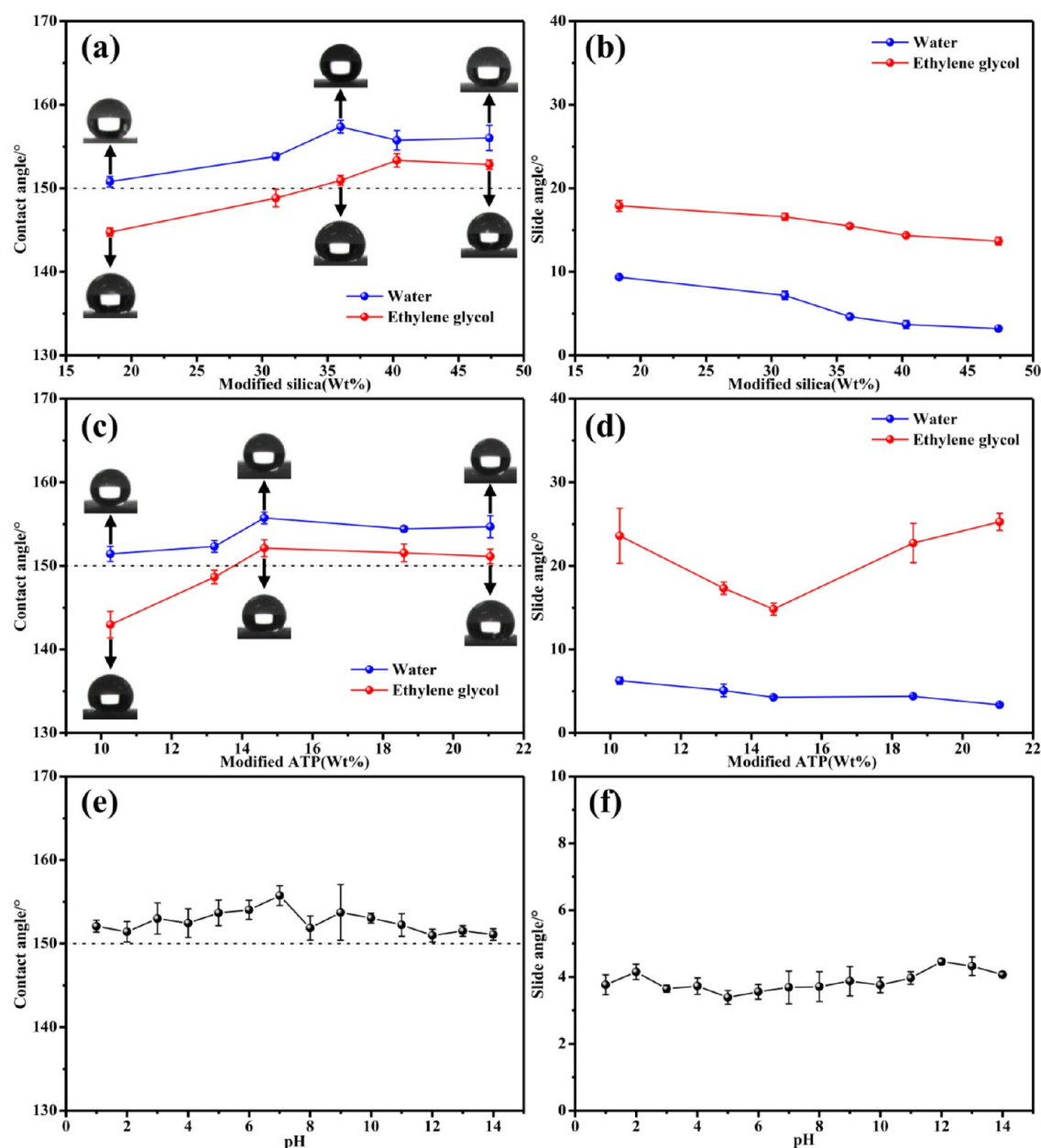


Figure 6. Wettability of the composite coating. (a, b) Effect of modified silica content on the wettability of the composite coating for water and ethylene glycol. (c, d) Effect of modified ATP content on the wettability of the composite coating for water and ethylene glycol. (e, f) CAs and SAs of the PTFE-ATP-SiO₂ composite coating to different pH solutions.

wt % (30 g) to 21.05 wt % (70 g), the CAs of water altered from $151 \pm 0.9^\circ$ to $156 \pm 0.7^\circ$, and the SAs of water decreased to less than 4° . However, when the weight percentage of modified ATP exceeded 14.63 wt % (45 g), the SAs of ethylene glycol were increased, and the CAs of ethylene glycol were decreased. Because when the weight percentage of modified ATP exceeded 14.63 wt % (45 g) in the coating system, the hydrophilicity and lipophilicity of modified ATP gradually appeared. Ten kinds of formulations were comprehensively considered, and the composite coating with 25 g of modified silica (90 wt %), 50 g of modified ATP (20 wt %), and 50 g of PTFE (60 wt %) obtained the best superamphiphobicity. Therefore, we chose the composite coating as the follow-up study and named it the PTFE-ATP-SiO₂ composite coating. When the modified ATP was 50 g and PTFE was 50 g, the coating was named the PTFE-ATP composite coating.

The PTFE-ATP-SiO₂ composite coating had high CAs and low SAs from pH 1 to 14 solution, proving that the PTFE-ATP-SiO₂ composite coating possessed good repulsion for corrosive droplets and prevented corrosive liquid from wetting the composite coating surface (Figure 6e,f). As a result, the PTFE-ATP-SiO₂ composite coating has a promising application in a corrosive environment.

3.4. Analysis of Morphology and Composition. As shown in Figure 7a, the surface of coating was prepared by spraying pure PTFE emulsion. Due to many voids, it was not conducive to anticorrosion of coating. Pure PTFE emulsion was mixed with modified ATP dispersion (20 wt %) to prepare the coating, which improved the compactness of coating and formed a continuous surface (Figure 7b). SEM images of the prepared PTFE-ATP-SiO₂ composite coating are shown in Figure 7c,d. It was obvious that the surface of the PTFE-ATP-

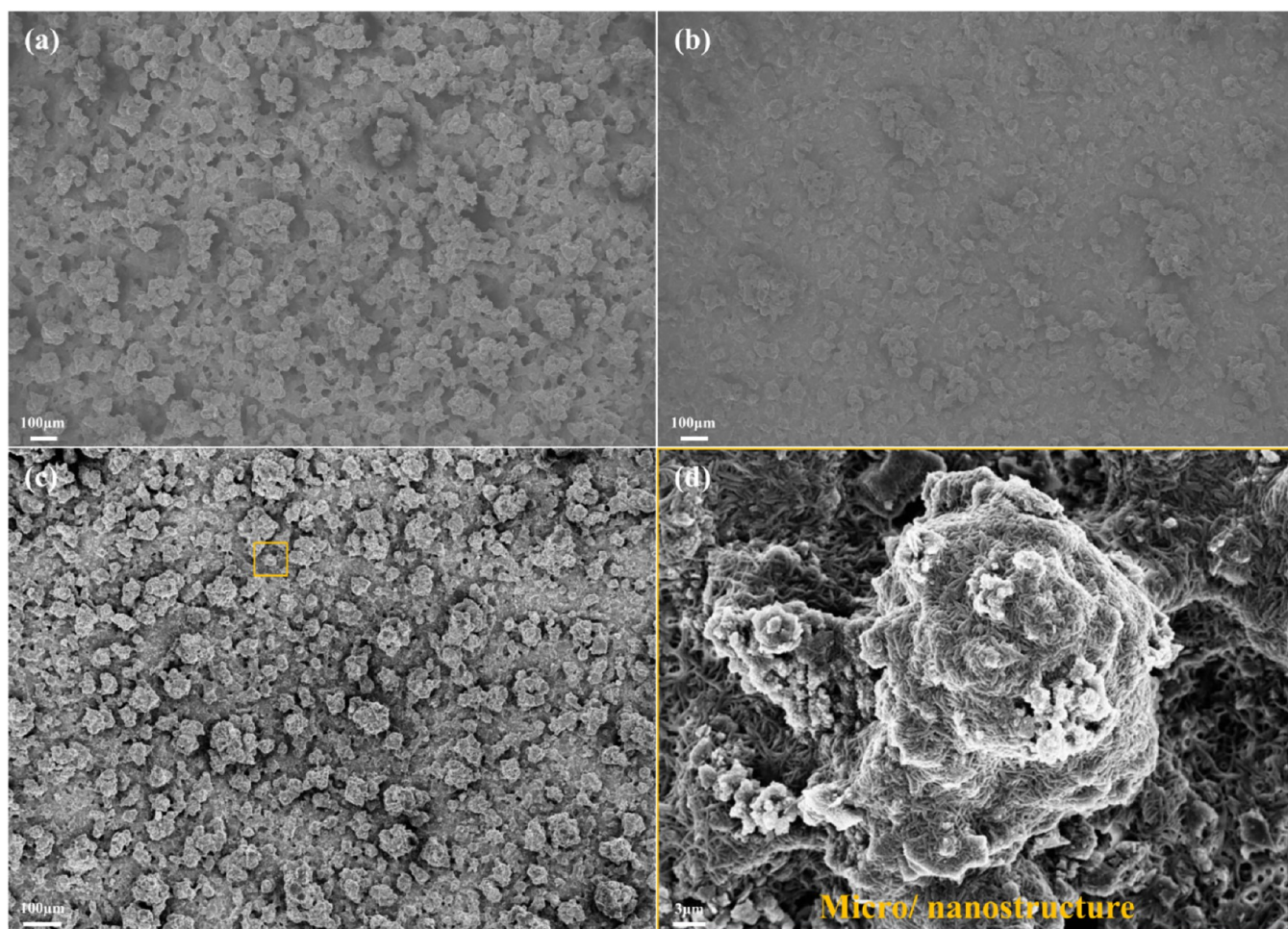


Figure 7. SEM of the composite coating. (a) SEM of pure PTFE coating. (b) SEM of the PTFE-ATP composite coating. (c, d) SEM of the PTFE-ATP-SiO₂ composite coating.

SiO₂ composite coating owned many hierarchical micro/nanostructures similar to the surface of lotus leaves. This structure intercepts air to form a stable gas film and enables the composite coating to show excellent water repellency.⁵¹ According to the surface scanning energy spectrum of the composite coating, it was composed of carbon, oxygen, fluorine, zinc, aluminum, silicon, and phosphorus (Figure 8a). The content of fluorine was the highest to reach 57.7 wt %, which provided low surface energy for the composite coating. The micro/nanostructures were also composed of these seven elements, and the content was basically the same as that of the composite coating surface (Figure 8c). From the element distribution (Figure 8b,d), it was clear that the elements were distributed uniformly in the composite coating surface, and the dispersibility of the prepared composite coating was excellent. As shown in Figure 9c, the PTFE-ATP-SiO₂ composite coating with 20 μm thickness was obtained after high-temperature curing (320 °C). The thickness of the film was obtained by measuring the height of the step at the junction of the substrate leak and the film (Figure 9b). The 3D surface morphology of the composite coating is shown in Figure 9a, and the arithmetic mean deviation of the profile (Ra) was 1.648 μm.

Compared with the infrared spectra and XRD phase analysis for modified ATP at normal atmospheric temperature, it was found that some changes have taken place in the infrared

spectra and XRD phase when modified ATP was kept at 320 °C (Figures S3 and S4). The corresponding diffraction peaks of AlPO₄ were found after high-temperature curing, but the corresponding diffraction peaks of H₂AlP₃O₁₀·H₂O and Zn₃(PO₄)₂·4H₂O were not found (Figures S5 and S6). It was also consistent with the infrared spectrum result; the peak at 424 cm⁻¹ (Zn–O) disappears (Figure S3 and Table S1). Moreover, the infrared spectra of PTFE were changed, but the XRD spectra were not changed at a high temperature of 320 °C for 20 min (Figures S3 and S4). These results affect the infrared spectra and XRD phase analysis of the PTFE-ATP-SiO₂ composite coating after high-temperature curing (Figures S3, S4, and S7).

3.5. Analysis of Self-Cleaning and Antipollution. A 10 min continuous rolling test (water and glycerol) and slurry dumping (45 wt %) test were executed to evaluate the antifouling performance of the PTFE-ATP-SiO₂ composite coating. The test results showed that the PTFE-ATP-SiO₂ composite coating had an excellent antipollution ability (Figure 10a–c). During the test (10 min), deionized water and glycerol were nearly spherical and quickly dripped (Movies S1 and S2). It still possessed high CAs for water after the 10 min continuous rolling test. It was worth mentioning that the slurry (45 wt %) was tested continuously for 10 min without any sediment invading the composite coating (Figure 10d and Movie S3). The CAs were 145 ± 0.5° for slurry, which showed

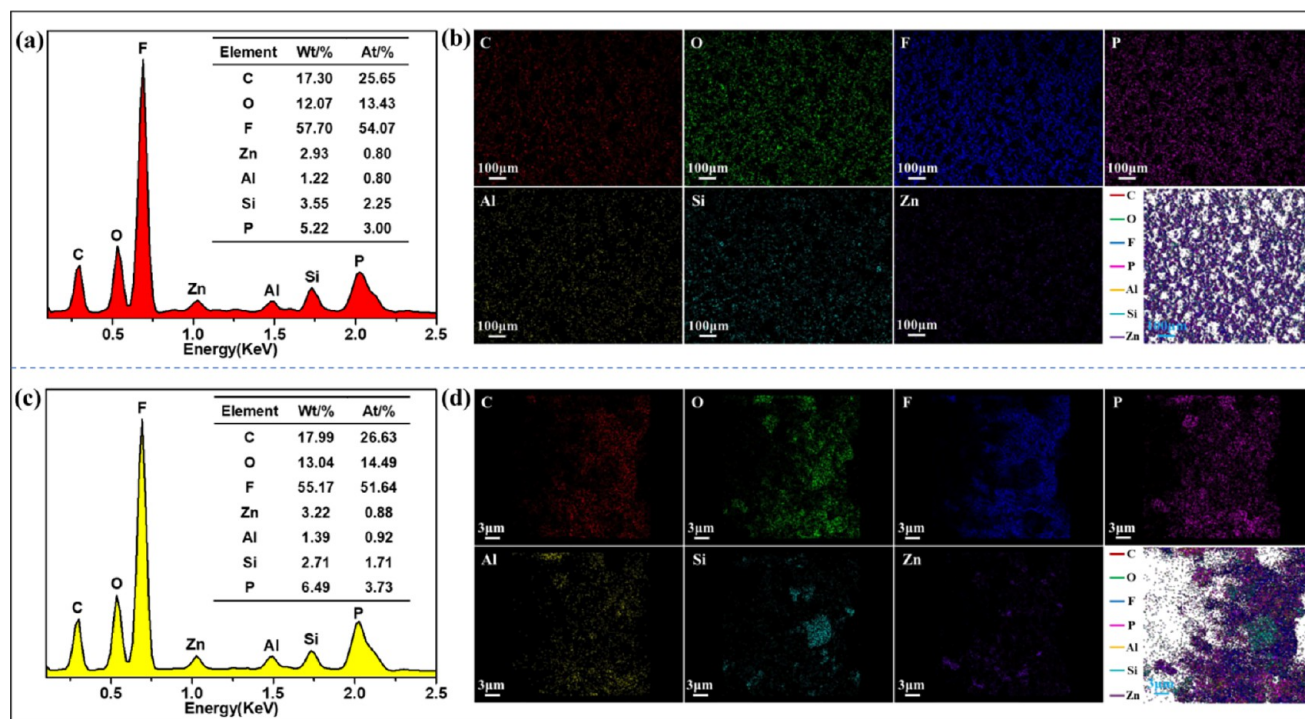


Figure 8. Element distribution of the composite coating. (a, b) Element content and element distribution of the PTFE-ATP-SiO₂ composite coating. (c, d) Element content and element distribution of emulsion protrusion.

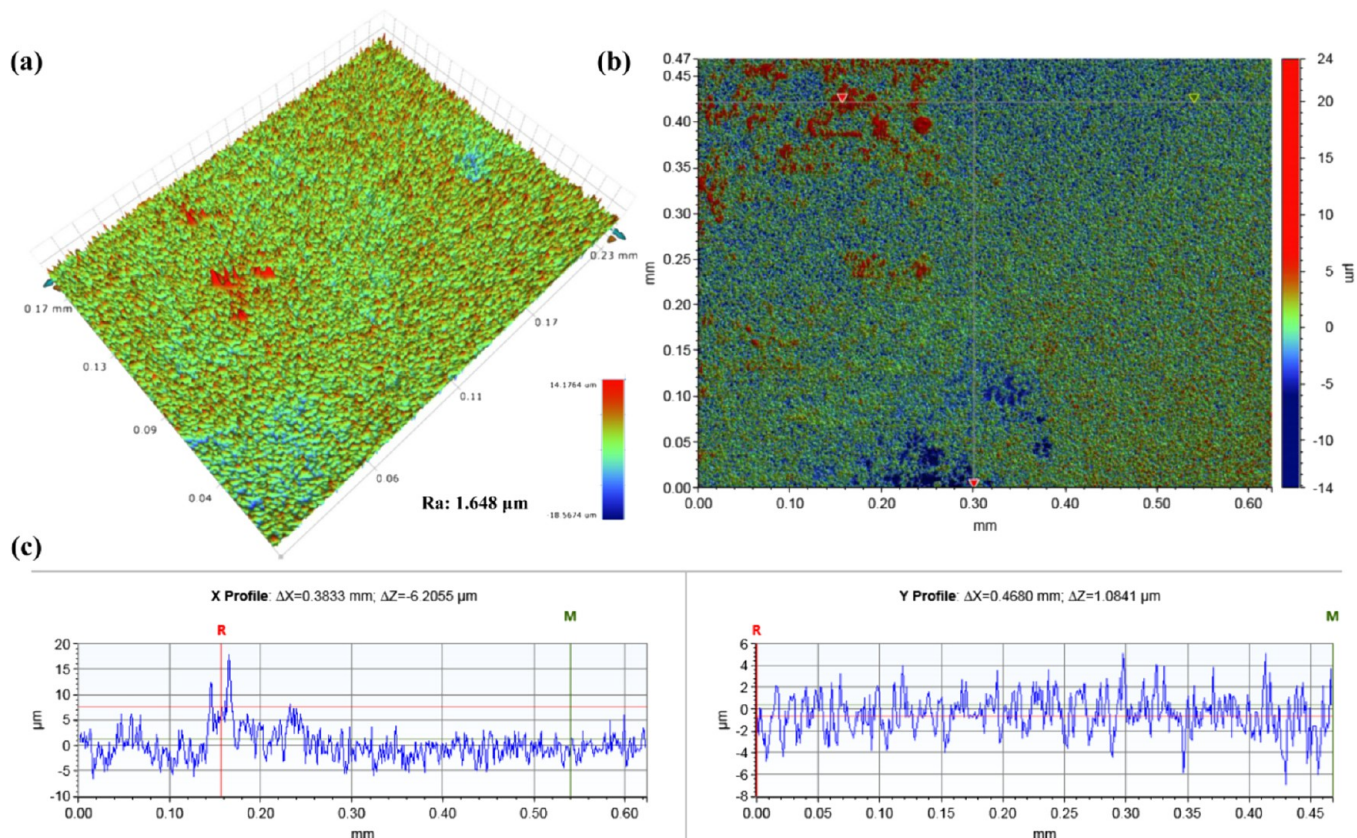


Figure 9. Morphology of the PTFE-ATP-SiO₂ composite coating. (a) 3D surface morphology of the composite coating. (b, c) Profile of the composite coating.

that the stability of the PTFE-ATP-SiO₂ composite coating was good. The self-cleaning performance of the PTFE-ATP-

SiO₂ composite coating needs to be observed. Silica and sand were placed on the coating surface, and then water drops fell

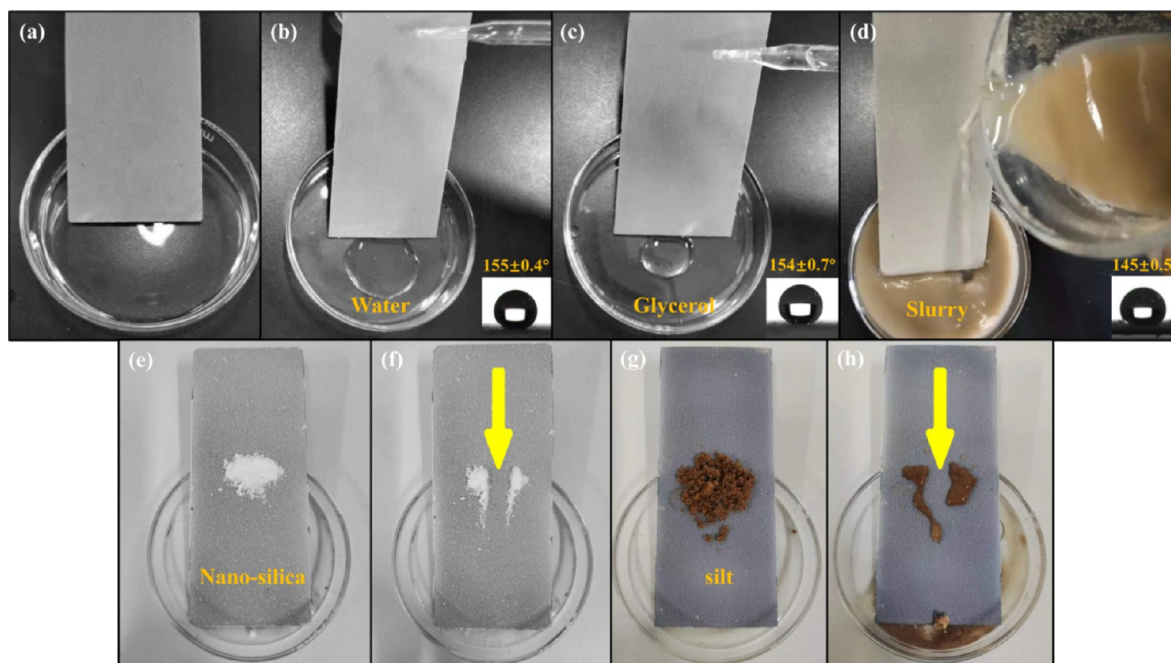


Figure 10. Self-cleaning and antipollution test. (a) PTFE-ATP-SiO₂ composite coating surface. (b) Deionized water test. (c) Glycerol test. (d) 45 wt % slurry test. (e, f) Self-cleaning test of silica. (g, h) Self-cleaning test of silt.

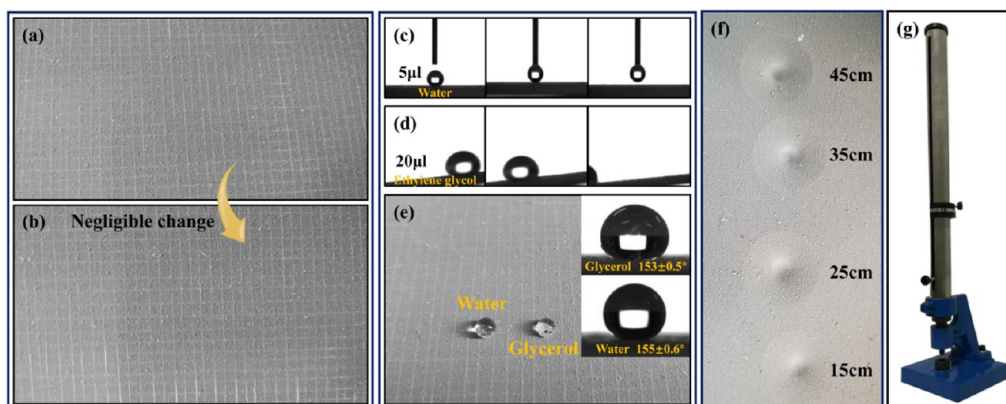


Figure 11. Mechanical property test. (a, b, e) Surface of the PTFE-ATP-SiO₂ composite coating before and after the cross-cut tape test. (c) Deionized water pull test. (d) Ethylene glycol rolling test. (f) The surface of the PTFE-ATP-SiO₂ composite coating was impacted by a heavy hammer at different heights. (g) The heavy hammer is a 1 kg coating impact instrument.

on the polluted area, which took away pollutants and formed a clean surface (Figure 10e–h). The PTFE-ATP-SiO₂ composite coating showed good self-cleaning performance. Therefore, the composite coating has good stability and self-cleaning performance, which are conducive to practical application.

3.6. Analysis of Mechanical Properties. The PTFE-ATP-SiO₂ composite coating was tested with a cross-cut tape test according to GB/T 9286 (Figure S8). The PTFE-ATP-SiO₂ composite coating was cut to a 1 mm × 1 mm grid by exposing the surface with a wallpaper knife and then pressed, and the 3M test tape was pulled until it was removed from the scored surface within 5 min, which was repeated three times. The peeling of scratch intersection after removal by the 3M test tape was neglected, and it was recognized as grade 1 adhesion (Figure 11a,b). After the cross-cut tape test, the composite coating still had high repellency for glycerol, ethylene glycol, and water (Figure 11d,e). Moreover, the composite coating surface still had an anti-adhesion ability

(Figure 11c). The impact resistance tester is shown in Figure 11g, and it evaluated the impact resistance of the PTFE-ATP-SiO₂ composite coating when a heavy hammer (1 kg) was dropped at different heights. The impact resistance of the composite coating was evaluated according to GB/T 1732-1993. The impact resistance was judged by observing the crack and peeling of the delamination ring on the surface of the composite coating. There was no crack on the surface of the PTFE-ATP-SiO₂ composite coating (Figure 11f) because of the high content of PTFE in the film-forming material and certain toughness after film formation. PTFE played a leading role in the PTFE-ATP-SiO₂ composite coating showing excellent impact resistance and good adhesion.

High-roughness sandpaper (120 mesh) was adhered on weights of different masses with double-sided adhesive, which was placed on the composite coating surface and pulled at constant speed. Then, it was pulled to the other side and returned to the original position again to record it once (Figure

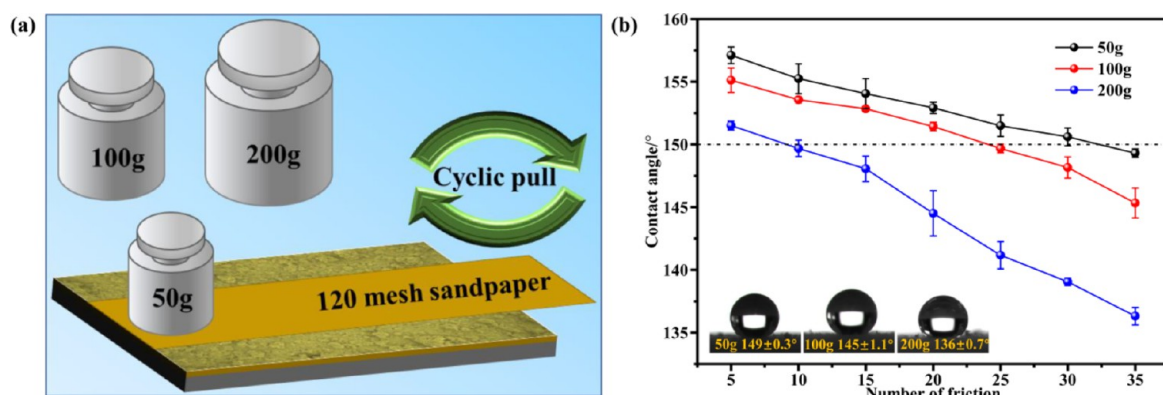


Figure 12. Abrasion resistance test. (a) Process of PTFE-ATP-SiO₂ composite coating wear resistance test. (b) Effect of different loads on the CAs.

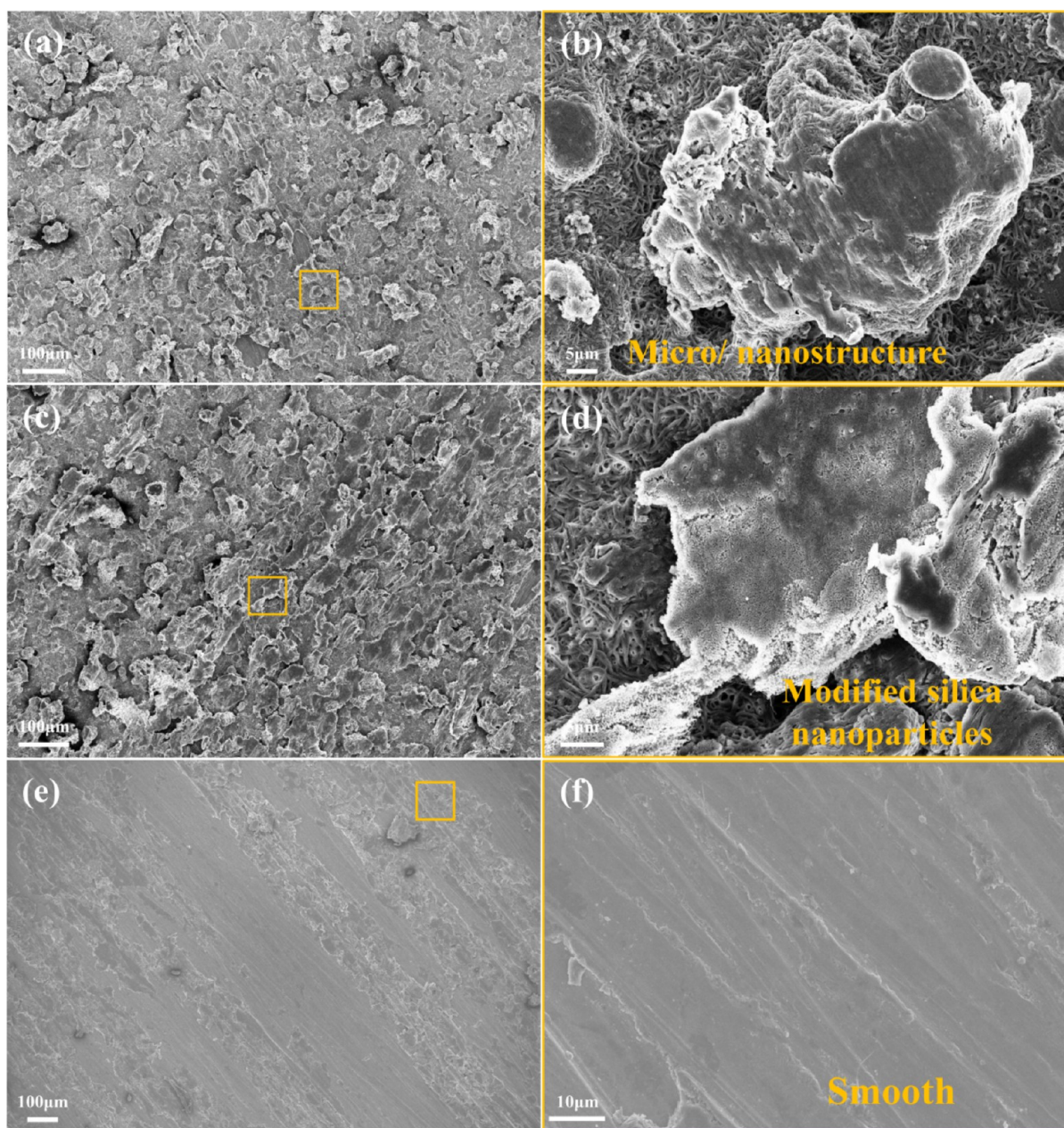


Figure 13. SEM of the PTFE-ATP-SiO₂ composite coating after the wear resistance test. (a, b) SEM of the composite coating after 35 cycles under 50 g loads. (c, d) SEM of the composite coating after 35 cycles under 100 g loads. (e, f) SEM of the composite coating after 35 cycles under 200 g loads.

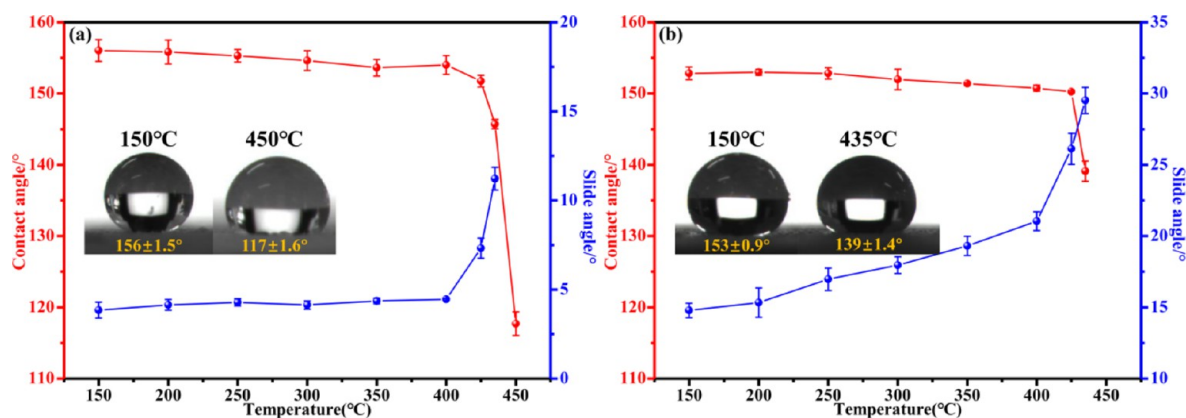


Figure 14. High temperature resistance test of the PTFE-ATP-SiO₂ composite coating. (a) Effect of heat treatment on CAs and SAs of water. (b) Effect of heat treatment on CAs and SAs of ethylene glycol.

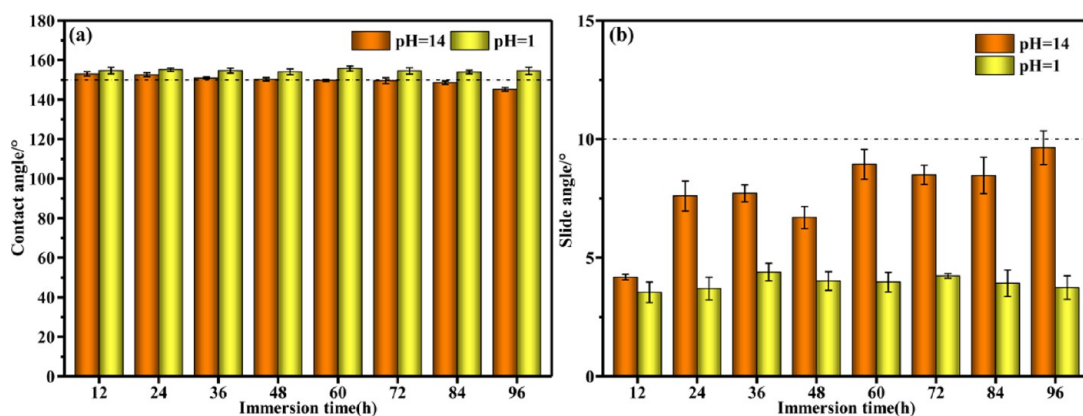


Figure 15. Acid–base immersion test. (a) CAs of the composite coating soaked in acid–base solution for different times. (b) SAs of the composite coating soaked in acid–base solution for different times.

12a). The CAs and SAs of the PTFE-ATP-SiO₂ composite coating were recorded every five times. The surface morphology of the PTFE-ATP-SiO₂ composite coating under 50 g loads is shown in Figure 13a,b; it was slightly damaged, the micro/nanostructures were also worn, and the CAs of deionized water were less than 150° after 35 cycles of wear. After 35 times of abrasion of the PTFE-ATP-SiO₂ composite coating under 100 g loads, it was found that the micro/nanostructures on the coating surface were ground flat, the modified silica in the composite coating was exposed (Figure 13c,d), and the CAs were reduced to 145 ± 1.1°. It was observed that the high-roughness surface of the PTFE-ATP-SiO₂ composite coating was completely polished after 35 times of wear under 200 g loads (Figure 13e), there were no micro/nanostructures (Figure 13f), and the CAs of water were reduced to 136 ± 0.7°. After 35 cycles of wear, compared with 50 g loads, the wear of the composite coating was intensified under 200 g loads. The micro/nanostructures disappeared and the rough surface was lost, which affected the surface wettability of the PTFE-ATP-SiO₂ composite coating. As shown in Figure 12b, the CAs of the PTFE-ATP-SiO₂ composite coating were decreased under three different loads, which intuitively proved the influence of micro/nanostructures and rough surface on hydrophobicity.^{52,53} Furthermore, the hardness of the PTFE-ATP-SiO₂ composite coating was grade 2B (Figure S9).

3.7. Analysis of Thermal Stability. For the sake of testing the thermal stability, coating annealing tests were carried out.

The wettability of the PTFE-ATP-SiO₂ composite coating after annealing for 1.5 h at different temperatures is shown in Figure 14. The CAs of the PTFE-ATP-SiO₂ composite coating decreased slightly with the increase in heat treatment temperature (within 425 °C) for water (CAs = 152 ± 0.8°; SAs = 7 ± 0.6°) and ethylene glycol (CAs = 150 ± 0.2°; SAs = 26 ± 1°). However, when the temperature exceeded 435 °C, the PTFE-ATP-SiO₂ composite coating lost superamphiphobicity. The results showed that the composite coating can maintain excellent thermal stability in a wide high-temperature range.

3.8. Analysis of Corrosion Resistance. The PTFE-ATP-SiO₂ composite coating was soaked in acid–base solution to evaluate the hydrophobicity and chemical stability. As shown in Figure 15, the change trend of the CAs and SAs was shown after soaking for different times in the environment of pH 1 and pH 14, respectively. The chemical stability of the composite coating was excellent for the hydrochloric acid solution with pH 1 (within 96 h). There was no significant change in the CAs and SAs of the composite coating before and after soaking, and the composite coating surface was not damaged (Figure 16a,b). Compared with hydrochloric acid solution with pH 1, the repellency of the composite coating was worse in KOH solution with pH 14. After soaking for 96 h, the CAs dropped to 145 ± 0.9°, and SAs increased to 10 ± 0.7°. It may be that with the increase in immersion time, the PTFE-ATP-SiO₂ composite coating contained acid-modified ATP that causes a chemical reaction with alkaline KOH,

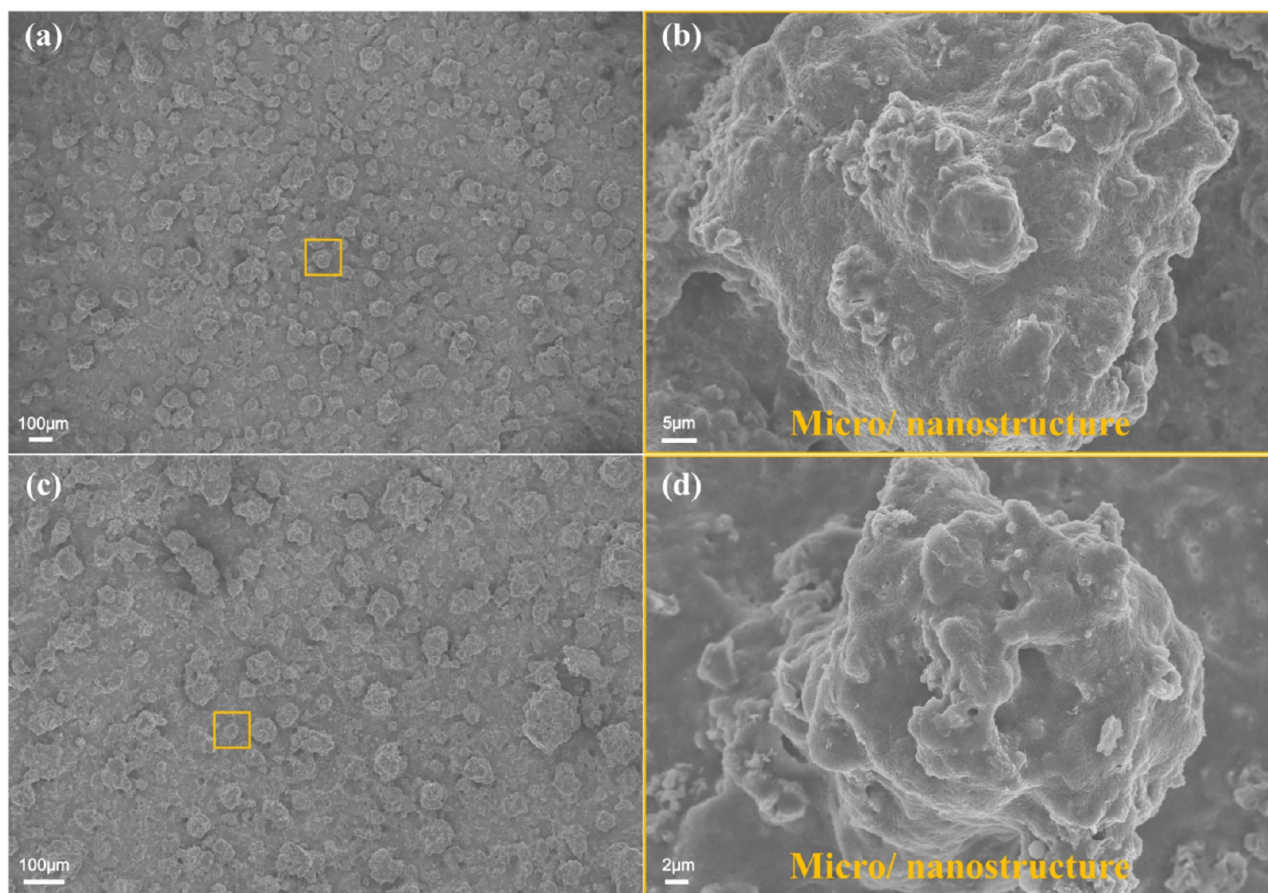


Figure 16. SEM of the PTFE-ATP-SiO₂ composite coating after the acid–base immersion test. (a, b) SEM of the composite coating after soaking in pH 1 solution for 96 h. (c, d) SEM of the composite coating after soaking in pH 14 solution for 96 h.

leading to the weakening of surface hydrophobicity. However, the morphology of the PTFE-ATP-SiO₂ composite coating had not changed significantly, and the micro/nanostructures had not been damaged (Figure 16c,d). Therefore, the composite coating possessed excellent chemical stability.

To explore the corrosion resistance of the PTFE-ATP-SiO₂ composite coating, it was soaked in 3.5 wt % NaCl solution to obtain Tafel plots and electrochemical impedance spectra (Figure 17). The relevant electrochemical parameters were obtained according to the polarization curve (Table 1). As shown in Figure 17a, compared with pure tinplate and PTFE coating, the PTFE-ATP coating had an E_{corr} positive shift, lower corrosion rate (-0.603 V), and higher protection efficiency (96.367%). It was attributed to the anticorrosive substance (modified ATP) and reduction of coating surface defects (Figure 7b). The corrosion resistance of the PTFE-ATP-SiO₂ composite coating was better than that of the PTFE-ATP coating due to the physical barrier in the composite coating (modified silica).

The corrosion rate (CR) and protection efficiency (PE) of the coating were obtained by corrosion current (I_{corr}) according to formulas 1 and 2.^{54,55}

$$\text{CR} = 3270 \times \frac{I_{\text{corr}} \cdot M}{V \cdot d} \quad (1)$$

$$\text{PE} = \left(1 - \frac{I_{\text{corr}}^c}{I_{\text{corr}}^0}\right) \quad (2)$$

) $\times 100$ where $3270 = 0.01 \times [1 \text{ year (in s)}/96,497.8]$ and $96,497.8 = 1 \text{ F}$ in Coulombs. Furthermore, V , M , and d represent the valence (+2), atomic mass (55.845), and density (7.85 g/cm^3) of the tinplate substrate, respectively. I_{corr}^0 and I_{corr}^c belong to the corrosion current of the bare tinplate substrate and the corrosion current of the coated tinplate substrate (determined by the intersection of the linear portions of the anodic and cathodic curves), respectively.

For the sake of exploring the long-term protection efficiency of the PTFE-ATP-SiO₂ composite coating, the polarization curves and electrochemical impedance spectra of the PTFE-ATP-SiO₂ composite coating at different times were obtained (Figure 17b).

As shown in Table 1, the PTFE-ATP-SiO₂ composite coating had the largest positive displacement, low corrosion rate, and high protection efficiency after soaking for 6 h. However, after soaking for 5 days, the polarization curve of the PTFE-ATP-SiO₂ composite coating had a slight negative shift compared with that of the coating soaking for 6 h. With the increase in immersion time, the degree of negative shift of the PTFE-ATP-SiO₂ composite coating polarization curve increased. After 20 days of immersion, the degree of negative shift (-0.605 V) was higher than that of the PTFE-ATP-SiO₂ composite coating soaked for 6 h, and the protection efficiency decreased to 89.1%. Electrochemical impedance spectroscopy was in good agreement with the polarization curve, which also proved that the corrosion resistance of the PTFE-ATP-SiO₂ composite coating was reduced (Figure 17c). With the increase in immersion time, the semicircle diameter of EIS decreased,

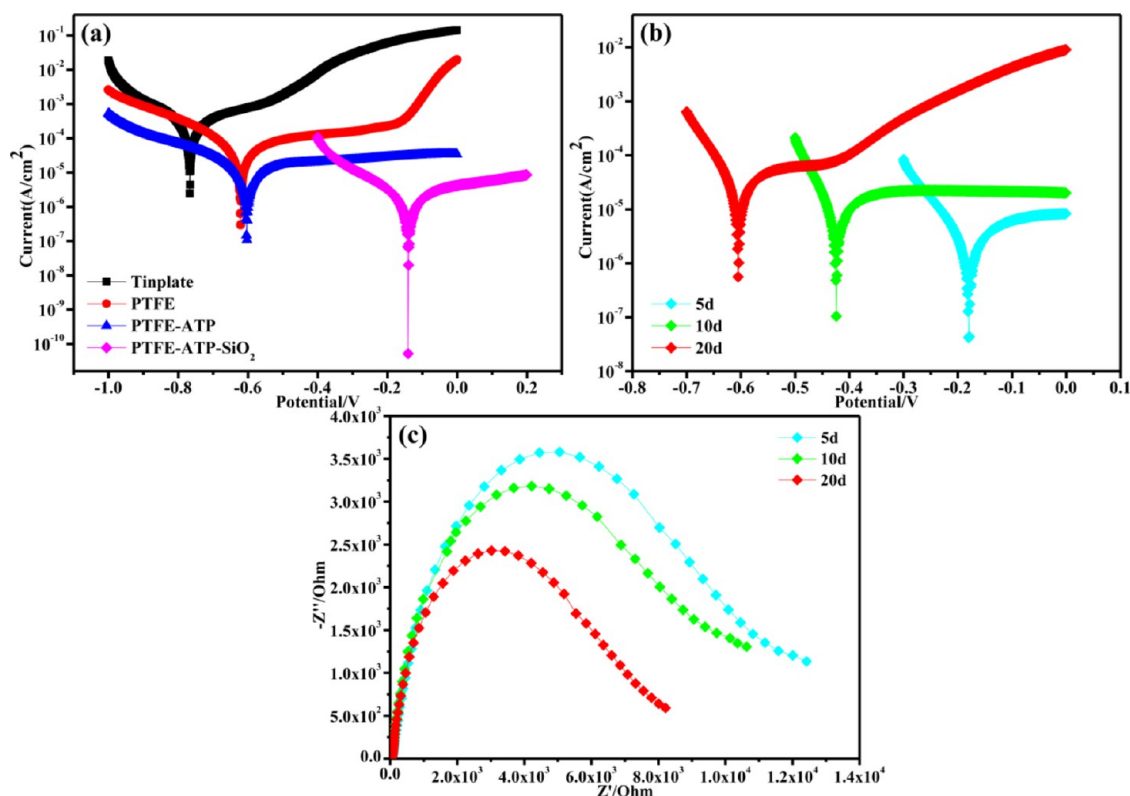


Figure 17. Corrosion resistance test. (a) Polarization curve test. (b) Polarization curve of the PTFE-ATP-SiO₂ composite coating for different times. (c) EIS of the PTFE-ATP-SiO₂ composite coating for different times.

Table 1. Polarization Values for Uncoated and Coated Tinplate Substrates

sample	immersion time	E_{corr} (V)	I_{corr} (A/cm ²)	CR ($\mu\text{m}/\text{year}$)	PE (%)
tinplate	6 h	-0.767	3.457×10^{-4}	4021	
PTFE	6 h	-0.621	2.620×10^{-5}	305	92.421
PTFE-ATP	6 h	-0.603	1.256×10^{-5}	146	96.367
PTFE-ATP-SiO ₂	6 h	-0.142	1.850×10^{-6}	21	99.465
PTFE-ATP-SiO ₂	5 days	-0.181	3.484×10^{-6}	40	98.992
PTFE-ATP-SiO ₂	10 days	-0.423	1.071×10^{-5}	125	96.902
PTFE-ATP-SiO ₂	20 days	-0.605	3.768×10^{-5}	438	89.100

and the protection efficiency decreased. The PTFE-ATP-SiO₂ composite coating had a long-term protection efficiency of 20 days, because the modified silica in the composite coating prolonged the time to reach the tinplate surface for corrosive substances. In addition, the air was intercepted by the rough structure of the composite coating to improve the corrosion resistance. Therefore, the PTFE-ATP-SiO₂ composite coating can be used in a corrosive environment.

4. CONCLUSIONS

In summary, modified silica dispersion was blended with PTFE emulsion and modified ATP dispersion to prepare an aqueous coating without introducing an external surfactant. The composite coating possessed good adhesion (grade 1), thermal stability (<425 °C), excellent antifouling, and impact resistance. More importantly, the superamphiphobic surfaces had obtained strong repulsion to ethylene glycol (CAs = $154 \pm 0.8^\circ$; SAs = $13 \pm 0.7^\circ$) and water (CAs = $158 \pm 0.7^\circ$; SAs = $4 \pm 0.3^\circ$). Under different loads (50, 100, and 200 g), the coating still possessed hydrophobicity after 35 cycles of wear of high-roughness sandpaper (120 mesh). Moreover, the

composite coating had long-term chemical stability to HCl solution (pH 1) and KOH (pH 14) solution for 96 h. The polarization curve and electrochemical impedance analysis showed that the PTFE-ATP-SiO₂ composite coating exhibited long-term corrosion resistance (20 days), which was mainly due to the superhydrophobicity of the composite coating and physical barrier effect. It is believed that the PTFE-ATP-SiO₂ composite coating has promising potential in the corrosion protection.

■ ASSOCIATED CONTENT

Supporting Information

The Supporting Information is available free of charge at <https://pubs.acs.org/doi/10.1021/acsomega.2c06859>.

Antipollution test for glycerol (Movie S1) (MP4)

Antipollution test for water (Movie S2) (MP4)

Antipollution test for slurry (Movie S3) (MP4)

Surface of the composite coating after redispersion (Figure S1); solid-liquid contact area fraction of the composite coating (Figure S2); FT-IR spectra (Figure S3); XRD spectra (Figure S4); XRD spectra of modified

ATP (Figure S5); XRD spectra of modified ATP held at a high temperature of 320 °C for 20 min (Figure S6); XRD spectra of the PTFE-ATP-SiO₂ composite coating (Figure S7); functional group details of the FT-IR spectra (Table S1); GB/T 9286 (Figure S8); SEM of the PTFE-ATP-SiO₂ composite coating after the hardness test (Figure S9) (PDF)

AUTHOR INFORMATION

Corresponding Author

Guoyu Ren – School of Chemistry and Chemical Engineering, Yulin University, Yulin, Shaanxi 719000, P. R. China; Shaanxi Yulin Energy Group Co., Ltd, Yulin, Shaanxi 719054, P. R. China; orcid.org/0000-0002-7683-7048; Email: rgy5617@163.com

Authors

Zeting Qiao – School of Chemistry and Chemical Engineering, Yulin University, Yulin, Shaanxi 719000, P. R. China

Zhi Hui – Yulin Sci-Tech Innovation New City, Yulin, Shaanxi 719000, P. R. China

Yun Tuo – School of Chemistry and Chemical Engineering, Yulin University, Yulin, Shaanxi 719000, P. R. China

Wenjie Zheng – School of Chemistry and Chemical Engineering, Yulin University, Yulin, Shaanxi 719000, P. R. China

Xiaodong Chen – School of Chemistry and Chemical Engineering, Yulin University, Yulin, Shaanxi 719000, P. R. China; orcid.org/0000-0003-3901-3434

Shiying Li – Yulin Energy Technology Operation Co., Ltd., of Cas, Yulin, Shaanxi 719000, P. R. China

Complete contact information is available at:

<https://pubs.acs.org/10.1021/acsomega.2c06859>

Notes

The authors declare no competing financial interest.

ACKNOWLEDGMENTS

The research is financially supported by the National Natural Science Foundation of China (21968036 and 22268046), Nature Scientific Research Foundation of Shaanxi Provincial Education Office of China (20JC040), Joint Fund Project of Yulin University-Dalian National Laboratory for Clean Energy (YLU-DNL2022005, 2021007, 2021016, and 2021018), Science and Technology Plan Project of Yulin City (CXY-2022-80), Science and Technology Plan Project of Yulin National High Tech Industrial Development Zone (CXY-2021-125 and YGXXG-2022-102), Advanced Talents Foundation of Yulin University (18GK19), and Science and Technology Innovation Leader Program of Shaanxi Provincial Science and Technology Department (2022SR2098), Post-graduate Teaching Materials Foundation of Yulin University (yjsjc201902).

REFERENCES

- (1) Liu, K.; Tian, Y.; Jiang, L. Bio-inspired superoleophobic and smart materials: Design, fabrication, and application. *Prog. Mater. Sci.* **2013**, *58*, 503–564.
- (2) Epstein, A. K.; Pokroy, B.; Seminara, A.; Aizenberg, J. Bacterial biofilm shows persistent resistance to liquid wetting and gas penetration. *Proc. Natl. Acad. Sci. U. S. A.* **2010**, *108*, 995–1000.
- (3) Rakitov, R.; Gorb, S. N. Brochosomal coats turn leafhopper (Insecta, Hemiptera, Cicadellidae) integument to superhydrophobic state. *Proc. R. Soc. B* **2012**, *280*, 20122391.
- (4) Lin, L.; Liu, M.; Chen, L.; Chen, P.; Ma, J.; Han, D.; Jiang, L. Bio-Inspired Hierarchical Macromolecule-Nanoclay Hydrogels for Robust Underwater Superoleophobicity. *Adv. Mater.* **2010**, *22*, 4826–4830.
- (5) Hensel, R.; Helbig, R.; Aland, S.; Voigt, A.; Neinhuis, C.; Werner, C. Tunable nano-replication to explore the omniphobic characteristics of springtail skin. *NPG Asia Mater.* **2013**, *5*, No. e37.
- (6) Hensel, R.; Neinhuis, C.; Werner, C. The springtail cuticle as a blueprint for omniphobic surfaces. *Chem. Soc. Rev.* **2016**, *45*, 323–341.
- (7) Si, W.; Guo, Z. Enhancing the lifespan and durability of superamphiphobic surfaces for potential industrial applications: A review. *Adv. Colloid Interface Sci.* **2022**, *310*, 102797–102797.
- (8) Kim, J. H.; Mirzaei, A.; Kim, H. W.; Kim, S. S. Novel superamphiphobic surfaces based on micro-nano hierarchical fluorinated Ag/SiO₂ structures. *Appl. Surf. Sci.* **2018**, *445*, 262–271.
- (9) Jiao, X.; Li, M.; Yu, X.; Wong, W. S. Y.; Zhang, Y. Oil-immersion stable superamphiphobic coatings for long-term super liquid-repellency. *Chem. Eng. J.* **2021**, *420*, 127606.
- (10) Wang, H.; Lu, H.; Zhang, X. Super-robust superamphiphobic surface with anti-icing property. *RSC Adv.* **2019**, *9*, 27702–27709.
- (11) Hu, Z.; Wang, H.; Zhu, Y.; Zhu, Y. Rapid development of thickness-controllable superamphiphobic coating on the inner wall of long narrow pipes. *AIChE J.* **2017**, *63*, 3636–3641.
- (12) Zhang, D.; Wu, G.; Li, H.; Cui, Y.; Zhang, Y. Superamphiphobic surfaces with robust self-cleaning, abrasion resistance and anti-corrosion. *Chem. Eng. J.* **2021**, *406*, 126753.
- (13) Pan, S.; Kota, A. K.; Mabry, J. M.; Tuteja, A. Superomniphobic Surfaces for Effective Chemical Shielding. *J. Am. Chem. Soc.* **2013**, *135*, 578–581.
- (14) Peng, J.; Yuan, S.; Geng, H.; Zhang, X.; Zhang, M.; Xu, F.; Lin, D.; Gao, Y.; Wang, H. Robust and multifunctional superamphiphobic coating toward effective anti-adhesion. *Chem. Eng. J.* **2022**, *428*, 131162.
- (15) Barthlott, W.; Neinhuis, C. Purity of the sacred lotus, or escape from contamination in biological surfaces. *Planta* **1997**, *202*, 1–8.
- (16) Neinhuis, C.; Barthlott, W. Characterization and Distribution of Water-repellent, Self-cleaning Plant Surfaces. *Ann. Bot.* **1997**, *79*, 667–677.
- (17) Darmanin, T.; Guittard, F. Superhydrophobic and superoleophobic properties in nature. *Mater. Today* **2015**, *18*, 273–285.
- (18) Tuteja, A.; Choi, W.; McKinley, G. H.; Cohen, R. E.; Rubner, M. F. Design Parameters for Superhydrophobicity and Superoleophobicity. *MRS Bull.* **2008**, *33*, 752–758.
- (19) Wang, X.; Hu, H.; Ye, Q.; Gao, T.; Zhou, F.; Xue, Q. Superamphiphobic coatings with coralline-like structure enabled by one-step spray of polyurethane/carbon nanotube composites. *J. Mater. Chem.* **2012**, *22*, 9624–9631.
- (20) Guo, K.; Wu, K.; Li, X.; Jiang, B.; Wu, Y.; Tian, S. Study on electrical properties of Nano SiO₂/Phenolic-resin Superamphiphobic composite insulation materials. *IOP Conf. Ser.: Mater. Sci. Eng.* **2019**, *677*, No. 022104.
- (21) Valipour, M.; Birjandi, F. C.; Sargolzaei, J.; Shahtahmassebi, N. Durable, superhydrophobic, superoleophobic and corrosion resistant coating on the stainless steel surface using a scalable method. *Appl. Surf. Sci.* **2013**, *283*, 636–647.
- (22) Qu, M.; Ma, X.; He, J.; Feng, J.; Liu, S.; Yao, Y.; Hou, L.; Liu, X. Facile Selective and Diverse Fabrication of Superhydrophobic, Superoleophobic-Superhydrophilic and Superamphiphobic Materials from Kaolin. *ACS Appl. Mater. Interfaces* **2017**, *9*, 1011–1020.
- (23) Yuan, R.; Wu, S.; Yu, P.; Wang, B.; Mu, L.; Zhang, X.; Zhu, Y.; Wang, B.; Wang, H.; Zhu, J. Superamphiphobic and Electroactive Nanocomposite toward Self-Cleaning, Antiwear, and Anticorrosion Coatings. *ACS Appl. Mater. Interfaces* **2016**, *8*, 12481–12493.
- (24) Pan, S.; Guo, R.; Björnalm, M.; Richardson, J. J.; Li, L.; Peng, C.; Bertleff-Zieschang, N.; Xu, W.; Jiang, J.; Caruso, F. Coatings

- super-repellent to ultralow surface tension liquids. *Nat. Mater.* **2018**, *17*, 1040–1047.
- (25) Li, M.; Li, Y.; Xue, F.; Jing, X. Water-based acrylate copolymer/silica hybrids for facile preparation of robust and durable superhydrophobic coatings. *Appl. Surf. Sci.* **2018**, *447*, 489–499.
- (26) Chatzigrigoriou; Manoudis, P. N.; Karapanagiotis, I. Fabrication of Water Repellent Coatings Using Waterborne Resins for the Protection of the Cultural Heritage. *Macromol. Symp.* **2013**, *331-332*, 158–165.
- (27) Aslanidou, D.; Karapanagiotis, I.; Lampakis, D. Waterborne Superhydrophobic and Superoleophobic Coatings for the Protection of Marble and Sandstone. *Materials* **2018**, *11*, 585.
- (28) Aslanidou, D.; Karapanagiotis, I.; Panayiotou, C. Superhydrophobic, superoleophobic coatings for the protection of silk textiles. *Prog. Org. Coat.* **2016**, *97*, 44–52.
- (29) Liu, M.; Mao, T.; Zhang, Y.; Wu, X.; Liu, F.; Yang, H.; Wang, J.; Zheng, C.; Zhao, X.; Wang, Z. General Water-Based Strategy for the Preparation of Superhydrophobic Coatings on Smooth Substrates. *Ind. Eng. Chem. Res.* **2017**, *56*, 13783–13790.
- (30) Karapanagiotis, I.; Grosu, D.; Aslanidou, D.; Aifantis, K. E. Facile Method to Prepare Superhydrophobic and Water Repellent Cellulosic Paper. *J. Nanomater.* **2015**, *2015*, 219013.
- (31) Khaskhoussi, A.; Calabrese, L.; Proverbio, E. Superhydrophobic Self-Assembled Silane Monolayers on Hierarchical 6082 Aluminum Alloy for Anti-Corrosion Applications. *Appl. Sci.* **2020**, *10*, 2656.
- (32) Zhang, B.; Zeng, Y.; Wang, J.; Sun, Y.; Zhang, J.; Li, Y. Superamphiphobic aluminum alloy with low sliding angles and acid-alkali liquids repellency. *Mater. Des.* **2020**, *188*, 108479.
- (33) Khodaei, M.; Shadmani, S. Superhydrophobicity on aluminum through reactive-etching and TEOS/GPTMS/nano- Al_2O_3 silane-based nanocomposite coating. *Surf. Coat. Tech.* **2019**, *374*, 1078–1090.
- (34) Xu, Z.; Qi, H.; Cheng, Y.; He, X. Nanocoating: Anti-icing superamphiphobic surface on 1060 aluminum alloy mesh. *Appl. Surf. Sci.* **2019**, *498*, 143827.
- (35) Zhang, B.; Xu, W.; Xia, D.; Huang, Y.; Zhao, X.; Zhang, J. Spray coated superamphiphobic surface with hot water repellency and durable corrosion resistance. *Colloids Surf., A* **2020**, *596*, 124750.
- (36) Li, Y.; Hu, T.; Li, B.; Wei, J.; Zhang, J. Totally Waterborne and Highly Durable Superamphiphobic Coatings for Anti-Icing and Anticorrosion. *Adv. Mater. Interfaces* **2019**, *6*, 1901255.
- (37) Parfitt, G. D. The role of the surface in the dispersion of powders in liquids. *Pure Appl. Chem.* **1981**, *53*, 2233–2240.
- (38) Parfitt, G. D. The dispersion of powders in liquids — an introduction. *Powder Technol.* **1977**, *17*, 157–162.
- (39) Hartley, P. A.; Parfitt, G. D. Dispersion of powders in liquids. 1. The contribution of the van der Waals force to the cohesiveness of carbon black powders. *Langmuir* **1985**, *1*, 651–657.
- (40) Ding, Z.; Li, Y. Y.; Xu, M. R.; Hong, X.; Hong, S. X.; Dong, B. Electrochemical properties of aluminum tripolyphosphate modified chemically bonded phosphate ceramic anticorrosion coating. *Constr. Build. Mater.* **2020**, *251*, 118874.
- (41) Lu, X.; Sun, S.; Fan, Q.; Pei, X.; Dun, Y.; Feng, X.; Zou, C.; Lu, W. Investigation of Protective Performance of a Mg-Rich Primer Containing Aluminum Tri-Polyphosphate on AZ91D Magnesium Alloy in Simulated Acid Rain. *Coatings* **2019**, *9*, 649.
- (42) Stöber, W.; Fink, A.; Bohn, E. Controlled growth of monodisperse silica spheres in the micron size range. *J. Colloid Interface Sci.* **1968**, *26*, 62–69.
- (43) Mousavi, M. A.; Hassanajili, S.; Rahimpour, M. R. Synthesis of fluorinated nano-silica and its application in wettability alteration near-wellbore region in gas condensate reservoirs. *Appl. Surf. Sci.* **2013**, *273*, 205–214.
- (44) Zhu, J.; Liao, K. A Facile Method for Preparing a Superhydrophobic Block with Rapid Reparability. *Coatings* **2020**, *10*, 1202.
- (45) Zhu, W.; Wu, Y.; Zhang, Y. Fabrication and characterization of superhydrophobicity ZnO nanoparticles with two morphologies by using stearic acid. *Mater. Res. Express.* **2019**, *6*, 1150d1.
- (46) Skoczylas, M.; Bocian, S.; Buszewski, B. Influence of silica functionalization by amino acids and peptides on the stationary phases zeta potential. *J. Chromatogr. A.* **2018**, *1573*, 98–106.
- (47) Dembek, M.; Bocian, S.; Buszewski, B. Solvent Influence on Zeta Potential of Stationary Phase—Mobile Phase Interface. *Molecules* **2022**, *27*, 968.
- (48) Belenkii, D. I.; Magomedov, T. M. Nanoparticle size and zeta potential express analysis in initial material's control at the enterprises of powder industry. *J. Phys.: Conf. Ser.* **2018**, *1134*, No. 012007.
- (49) Xu, G.; Zhang, J.; Song, G. Effect of complexation on the zeta potential of silica powder. *Powder Technol.* **2003**, *134*, 218–222.
- (50) Cassie, A. B. D.; Baxter, S. Wettability of porous surfaces. *Trans. Faraday Soc.* **1944**, *40*, 546–551.
- (51) Koch, K.; Bhushan, B.; Jung, Y. C.; Barthlott, W. Fabrication of artificial Lotus leaves and significance of hierarchical structure for superhydrophobicity and low adhesion. *Soft Matter* **2009**, *5*, 1386–1393.
- (52) Feng, L.; Li, L.; Li, Y.; Li, H.; Zhang, L.; Zhai, J.; Song, Y.; Liu, B.; Jiang, L.; Zhu, D. Superhydrophobic Surfaces: From Natural to Artificial. *Adv. Mater.* **2002**, *14*, 1857–1860.
- (53) Bhushan, B.; Koch, K.; Jung, Y. C. Nanostructures for superhydrophobicity and low adhesion. *Soft Matter* **2008**, *4*, 1799–1804.
- (54) Yuan, R.; Wu, S.; Wang, B.; Liu, Z.; Mu, L.; Ji, T.; Chen, L.; Liu, B.; Wang, H.; Zhu, J. Superamphiphobicity and electroactivity enabled dual physical/chemical protections in novel anticorrosive nanocomposite coatings. *Polymer* **2016**, *85*, 37–46.
- (55) Madhan, K.; Gasem, Z. M. In situ electrochemical synthesis of polyaniline/f-MWCNT nanocomposite coatings on mild steel for corrosion protection in 3.5% NaCl solution. *Prog. Org. Coat.* **2015**, *78*, 387–394.